NANO LETTERS
Cite This: Nano Lett. 2018, 18, 6347−6352
Letter
pubs.acs.org/NanoLett

Control of Epitaxial $BaFe_2As_2$ Atomic Configurations with Substrate Surface Terminations

Jong-Hoon Kang,[†] Lin Xie,[‡,§,○] Yi Wang,[∥] Hyungwoo Lee,[†] Neil Campbell,[⊥] Jianyi Jiang,[#] Philip J. Ryan,[▽] David J. Keavney,[▽] Jung-Woo Lee,[†] Tae Heon Kim,[†] Xiaoqing Pan,[‡] Long-Qing Chen,[∥] Eric E. Hellstrom,[#] Mark S. Rzchowski,[⊥] Zi-Kui Liu,[∥] and Chang-Beom Eom*[,†]

[†]Department of Materials Science and Engineering, University of Wisconsin-Madison, Madison, Wisconsin 53706, United States
[‡]Department of Materials Science and Engineering and Department of Physics and Astronomy, University of California-Irvine, Irvine, California 92679, United States
[§]National Laboratory of Solid State Microstructures and College of Engineering and Applied Sciences, Nanjing University, Nanjing, Jiangsu 210093, People's Republic of China
[∥]Department of Materials Science and Engineering, The Pennsylvania State University, University Park, Pennsylvania 16802, United States
[⊥]Department of Physics, University of Wisconsin-Madison, Madison, Wisconsin 53706, United States
[#]Applied Superconductivity Center, National High Magnetic Field Laboratory, Florida State University, 2031 East Paul Dirac Drive, Tallahassee, Florida 32310, United States
[▽]Advanced Photon Source, Argonne National Laboratory, Argonne, Illinois 60439, United States

Supporting Information

ABSTRACT: Atomic layer controlled growth of epitaxial thin films of unconventional superconductors opens the opportunity to discover novel high temperature superconductors. For instance, the interfacial atomic configurations may play an important role in superconducting behavior of monolayer FeSe on $SrTiO_3$ and other Fe-based superconducting thin films. Here, we demonstrate a selective control of the atomic configurations in Co-doped $BaFe_2As_2$ epitaxial thin films and its strong influence on superconducting transition temperatures by manipulating surface termination of (001) $SrTiO_3$ substrates. In a combination of first-principles calculations and high-resolution scanning transmission electron microscopy imaging, we show that Co-doped $BaFe_2As_2$ on TiO_2-terminated $SrTiO_3$ is a tetragonal structure with an atomically sharp interface and with an initial Ba layer. In contrast, Co-doped $BaFe_2As_2$ on SrO-terminated $SrTiO_3$ has a monoclinic distortion and a $BaFeO_{3-x}$ initial layer. Furthermore, the superconducting transition temperature of Co-doped $BaFe_2As_2$ ultrathin films on TiO_2-terminated $SrTiO_3$ is significantly higher than that on SrO-terminated $SrTiO_3$, which we attribute to shaper interfaces with no lattice distortions. This study allows the design of the interfacial atomic configurations and the effects of the interface on superconductivity in Fe-based superconductors.

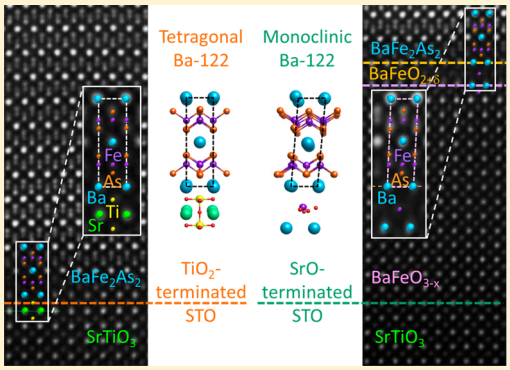

KEYWORDS: *Superconducting T_c, $BaFe_2As_2$, interfacial atomic structure, surface termination, thin films, heterostructures*

The discovery of high-temperature superconductivity in Fe-based compounds[1] has sparked intense research activity[2−8] to understand the mechanisms of the superconductivity and enhance the superconducting critical temperature (T_c). It has been reported that T_c is very sensitive to small changes of atomic structure, for instance, from perturbations such as the pnictogen (P, As) or chalcogen (S, Se, Te) anions, and hydrostatic pressure.[8−15] Thin films provide another route to comprehensive control of the atomic structure for the further enhancement of T_c because unlike in bulk both tensile and compressive biaxial strain can be applied easily.[16,17] The dimensionality of the material is decreased from 3D to 2D which also opens the opportunity to study the mechanism that gives rise to the enhancement of the critical temperature. For instance, well-known Fe-based superconductor, monolayer FeSe on $SrTiO_3$ shows a 10 times enhancement of T_c over the bulk.[18−23] Despite the strong influence of atomic structure on T_c, there lacks a comprehensive study of interfacial atomic structure control and the concomitant superconducting T_c in thin film heterostructures. To make progress, it is crucial to control atomic configurations near the interface between Fe-based superconductors and substrates.

Received: July 3, 2018
Revised: August 9, 2018
Published: August 27, 2018

DOI: 10.1021/acs.nanolett.8b02704
Nano Lett. 2018, 18, 6347−6352

$BaFe_2As_2$ (Ba-122)/$SrTiO_3$ (STO) heterostructure is an excellent platform to explore the relationship between atomic structure and superconducting T_c in thin films because of good lattice matching, chemical/electronic compatibility, and chemical stability to air exposure.[4,24−28]

Here, we report selective control of the atomic configurations in Co-doped $BaFe_2As_2$ epitaxial thin films by manipulating the surface termination of (001) $SrTiO_3$ substrates, and the strong influence of these configurations on superconducting transition temperatures. Three different substrate terminations, namely, pure TiO_2-terminated,[29] SrO-terminated, and mixed TiO_2/SrO-terminated STO substrates were used to grow Co-doped Ba-122 thin films by pulsed laser deposition with a KrF (248 nm) ultraviolet excimer laser at 730 °C (growth rate: 2.4 nm/sec). The STO substrates were attached to a resistively heated block with silver paste in a growth chamber with base pressure 3×10^{-5} Pa. After the film growth, the heater was slowly cooled by removing the heater power (see Supporting Information for details). The atomic structures at the interfaces with different surface terminations were investigated by high-resolution scanning transmission electron microscopy (HR-STEM) and compared to density functional theory calculations. We find that surface termination control can significantly improve interfacial sharpness, leading to a higher T_c in the Ba-122 grown on TiO_2-termination than that of distorted Ba-122 on SrO-termination.

Dependence of Interface Structure on Substrate Termination. We performed atomic-resolution STEM high-angle annular dark-field (HAADF) imaging and electron energy loss spectroscopy (EELS) experiments on a double aberration-corrected transmission electron microscope FEI Titan 60-300 to investigate atomic arrangements and chemical diffusion at the heterointerfaces (Figure 1). Images were averaged along the interface to improve the signal-to-noise ratio (see Supporting Information for details). Figure 1a,b shows the averaged STEM HAADF images of Ba-122 on TiO_2- and SrO-terminated STO, respectively. They show clear evidence that atomic structures at the heterointerfaces are selectively controlled by the surface terminations of STO (Figure S1 in Supporting Information).

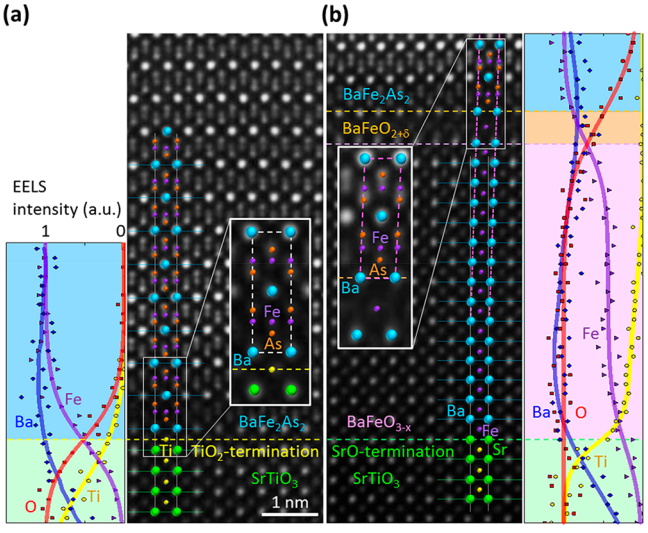

Figure 1. High-resolution STEM HAADF images and EELS profiles of Ba-122/STO heterostructures with (a) TiO_2- and (b) SrO-terminations. Atomic structures were imaged along the [100] zone axis. EELS vertical line scan across the interface of Ba-122/STO with steps of ~0.2 nm along the [001] direction.

On TiO_2-terminated STO, one unit-cell of $BaFe_2As_2$ consists of a stacked structure of Ba−AsFeAs−Ba−AsFeAs−Ba (white box in Figure 1a), where at the interface the Ba atom is aligned with Sr along the vertical direction (white dotted line in Figure 1a). There is no significant structural distortion in the Ba-122 film, and the heterointerface is atomically sharp. The reduced contrast of the first Ba atomic layer with the STO could be due to cation interdiffusion of Ba and Sr or atomic reconstructions at the interface, as is suggested by the elongation of the contrast for each Ba/Sr atom along the growth direction.

Contrary to the TiO_2-termination, a monoclinic structural distortion was found near the interfacial region of the SrO-terminated STO (Figure 1b). First of all, the stacking of Ba−AsFeAs−Ba is not seen at the interface, but a repeating stacking sequence of FeO_2−BaO appears in the STEM HAADF image. Therefore, $BaFeO_{3-x}$ is directly grown on the SrO-termination, accompanied by O diffusion from the STO substrate (red line of EELS scan in the pink region of the interfacial layer). More interestingly, we found the monoclinic distortion of $BaFeO_{3-x}$, shown by the vertical pink dashed line in the STEM image. The monoclinic phase of $BaFeO_{2.5}$ has been reported previously,[30,31] resulting from oxygen deficiency favoring the oxidation states of Fe^{3+}. As is shown in Figure S2, the onset energies of Fe-$L_{2,3}$ edge in the interfacial layer are systematically shifted to lower energy-losses as the vertical position is farther away from the substrate. A higher onset energy indicates a higher oxidation state of Fe^{4+} near the $BaFeO_{3-x}$/$SrTiO_3$ interface,[32] while a lower onset energy suggests a lower oxidation state of Fe^{2+}/Fe^{3+} in $BaFeO_{2+\delta}$ and $BaFe_2As_2$. In addition to oxidation states, we investigated the fine structure of Ti-$L_{2,3}$ edge and O-K edge of STO showing strong multiple peaks arising from the octahedral coordination of Ti atoms in cubic STO.[33] However, we do not observe strong multiple peaks in Fe-$L_{2,3}$ and O-K edge EELS spectra of $BaFeO_{3-x}$ (Figure S2 in Supporting Information). This might indicate that the Fe atom is in a distorted octahedral coordination due to monoclinic distortion of $BaFeO_{3-x}$.

The monoclinic $BaFeO_{3-x}$ at the SrO-termination layer transits to a monolayer $BaFeO_{2+\delta}$ when oxygen is insufficient, and then monoclinic Ba-122 grows on the oxygen-deficient $BaFeO_{2+\delta}$ layer (Figure 1b). The atomic structure of the $BaFeO_{2+\delta}$ is also monoclinic, affected by the underlying $BaFeO_{3-x}$. Unlike $BaFeO_{3-x}$, the atomic structure of $BaFeO_{2+\delta}$ is elongated along the vertical direction, which replicates itself in the half unit cell of the following Ba-122 layer. The image of $BaFeO_{2+\delta}$ appears blurred due to chemical rearrangement of the Fe and O atoms resulting in disorder. Arsenic atom can be placed on top of the oxygen-deficient $BaFeO_{2+\delta}$ due to long diffusion distance approximately 3 nm away from the STO substrate. As a result, Ba-122 is finally synthesized on top of the $BaFeO_{2+\delta}$ because the oxide layer is no longer stable in the lack of oxygen. The structure of Ba-122 is still monoclinic (white box), influenced by the underneath $BaFeO_{2+\delta}$ (Figure S3 in Supporting Information).

Figure 2 shows a schematic comparison of interfacial atomic configurations in the Ba-122 grown on TiO_2- and SrO-terminations of STO substrates. The Ba-122 film grown on TiO_2-terminated STO substrate shows an atomically sharp interface between Ba-122 film and the STO substrate (Figure 2a). Note that bulk Ba-122 superconductor has a tetragonal structure. The tetragonal structure with the atomically sharp

DOI: 10.1021/acs.nanolett.8b02704
Nano Lett. 2018, 18, 6347−6352

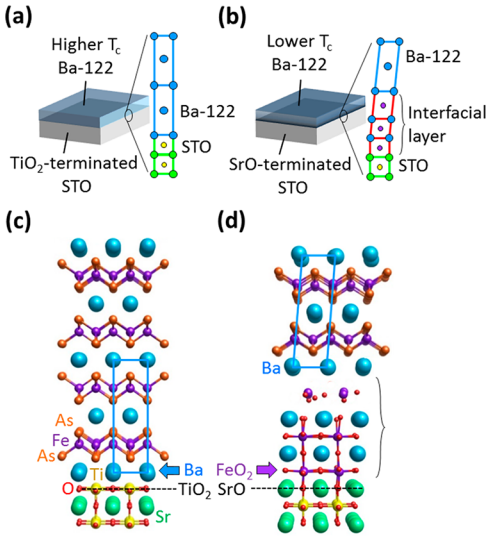

Figure 2. Schematic picture of distinct superconducting T_c of Co-doped Ba-122 film depending on (a) TiO_2 and (b) SrO surface terminations of (001) STO substrates. Growth models and atomic configurations of Ba-122 at the heterointerfaces with (c) TiO_2- and (d) SrO-terminations.

interface is observed in Ba-122 grown on TiO_2-terminated $SrTiO_3$ substrate. On the other hand, the interfacial layer shows strong disorder on the SrO-terminated STO causing the Ba-122 film to show the monoclinic phase (Figure 2b). Controlling interfacial structure via surface terminations enhances superconducting T_c in the Ba-122/STO heterostructures.

Calculations of Initial Growth on Different Termination Layers. We propose systematic growth models of Ba-122 on both TiO_2- and SrO-terminations (Figure 2c,d). We determine which layer is thermodynamically stable as the first layer on TiO_2 or SrO, and then consider whether the first layer has any preference to preserve or change perovskite oxide structure. First-principles calculations were performed to predict the most stable phases on TiO_2- and SrO-terminations (Table S1 in Supporting Information). To find the most stable interfacial structures between Ba-122 and STO, we have first designed 14 possible interfacial configuration models within the supercell approach. Phase stability was determined by comparing the total energy of a given structure with a convex hull construction based on the total energies of the 14 possible configurations together with energies for structures of pure elements As, Fe, Ba, and Sr and simple compounds BaO, Fe_2O_3, TiO_2, SrO, $SrTiO_3$, and $BaFe_2As_2$. The theoretical calculations show the Ba layer, instead of BaO, is energetically more favorable on TiO_2, and then Ba−AsFeAs−Ba stacking is stable with the tetragonal structure (Figure 2c). Contrary to the TiO_2-termination, FeO_2 is more stable than Fe on SrO to keep oxide structure (Figure 2d). We suggest $BaFeO_3$ (FeO_2−BaO) is grown on top of SrO, assisted by oxygen diffusion from the STO substrate, and eventually a Ba layer will be grown to form Ba-122 (Table S1 in Supporting Information). The atomic configurations determined by theoretical calculations are consistent with the experimental observations discussed in the previous section.

Transport Properties. In addition to the local atomic structures, we have studied the influence of TiO_2/SrO surface coverage of the surface terminations on the superconducting T_c of Co-doped Ba-122 films (Figure 3). We prepared pure TiO_2-termination and mixed surface termination (as-received),

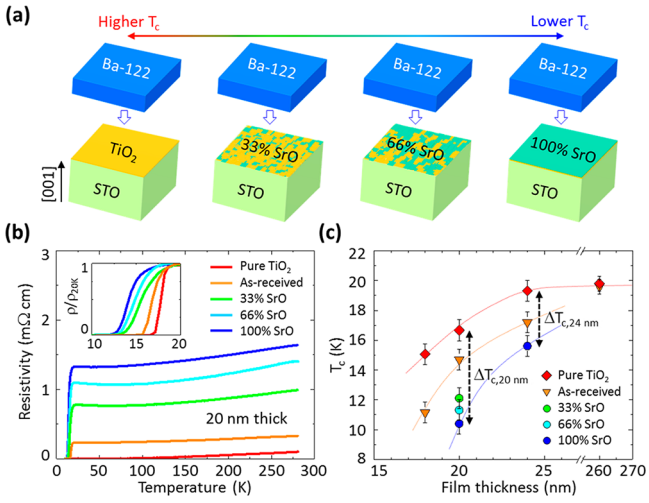

Figure 3. (a) Surface termination design for controlling superconducting T_c of Co-doped Ba-122 film. (b) Temperature-dependent resistivity and superconducting transition (inset), controlled by TiO_2/SrO. (c) Thickness-dependent T_c trend of Ba-122 film on different TiO_2/SrO surface coverage.

and also changed TiO_2/SrO ratio by growing SrO layer on pure TiO_2 surface. With in situ reflective high energy electron diffraction (RHEED) technique, the fraction of SrO surface was controlled by the number of laser pulses (Figure S4 in Supporting Information). We state 100% SrO coverage where the intensity of the RHEED oscillation is recovered at a local maximum value in one oscillation period and determine the percentage of SrO coverage based on number of pulses. Typically, it has been reported that the long-range nanoscale patterns of mixed-terminations in perovskite oxide substrates severely affect the growth of epitaxial films,[34] and therefore, the relevant length scales of mixed-terminations can impact on superconducting T_c. On the basis of our structural investigation, we expect higher-T_c from Ba-122 films with more TiO_2-termination (Figure 3a).

Temperature-dependent resistivity measurements (Figure 3b) of Co-doped Ba-122 show that the TiO_2/SrO terminations of the STO substrate affect the temperature dependent resistivity and the resistive T_c. In general, the overall resistivity decreases as the TiO_2/SrO termination ratio increases. We compared the residual resistivity ratio (RRR) to evaluate the scattering sources in Ba-122 films. The RRR is enhanced from 1.2 to 1.4 when the TiO_2:SrO ratio is higher, indicating less defect scattering in the Ba-122 film on TiO_2-termination (Figure S5 in Supporting Information), in good agreement with the STEM results. X-ray diffraction also shows Ba-122 grown on TiO_2 has narrower full width half-maximum (fwhm) of the (004) reflection rocking curve indicating better epitaxial quality of the films (Figure S6 in Supporting Information). Even though there might be the difference of local strain near grain boundaries due to monoclinic distortion in nanoscale regions, there is no overall strain effect because the STO substrates all have the same lattice parameters. There is however an influence of distortions in the interfacial layer on the atomic structure of Ba-122 films and interdiffusion into the films. Therefore, the proximity to TiO_2-termination reduces

DOI: 10.1021/acs.nanolett.8b02704
Nano Lett. 2018, 18, 6347−6352

scattering due to the structural imperfection near the interface and eventually enhances T_c (inset of Figure 3b).

Dependence of T_c on Film Thickness and Substrate Termination. We also demonstrate that the superconducting T_c depends on the TiO_2/SrO termination of STO (Figure 3c). T_c is enhanced as TiO_2/SrO ratio increases, and the variation of T_c with substrate termination (ΔT_c) significantly increases with the reduction of film thickness. The 260 nm thick film shows no T_c reduction from pure TiO_2 or from the as-received substrate, presumably because the disordered region nearby the interface is only a small portion of the thick film. No discernible differences in X-ray diffraction peak fwhm between the Ba-122 films grown on these two different substrates could be found at 260 nm (Figure S6 in Supporting Information). However, the T_c trend clearly shows the ΔT_c between pure TiO_2 and SrO is 3.7 K for a 24 nm thick film, and it increases to 6.3 K at 20 nm thickness. Our superconducting quantum interference device (SQUID) measurement of the magnetization T_c also show significant dependence on surface termination (Figure S7 in Supporting Information).

Figure 3c shows several interesting trends with film thickness and substrate termination. For the pure TiO_2-terminated STO, the superconducting T_c remains fairly high even in films as thick as 24 nm. We attribute the decreasing T_c to increased scattering in thinner Ba-122 films. Even TiO_2-termination shows T_c decreasing trend with decreasing film thickness. This gradual degradation of superconducting T_c at reduced dimensions might be related to chemical intermixing at the interface. However, in the case of SrO-termination T_c drops faster with decreasing thickness. We attribute this to a larger interfacial scattering due to larger fraction of the disordered $BaFeO_{3-x}$ and the distorted Ba-122 in thinner films. Therefore, the different thickness-dependent T_c between TiO_2- and SrO-terminations is caused by both the effective Ba-122 thickness and the epitaxial quality of Ba-122. Proximity effect may play a minor role, possibly arising from a weak magnetic ordering in the distorted $BaFeO_{3-x}$ We identified a very small magnetic signal in the Fe-$L_{2,3}$ edge X-ray magnetic circular dichroism spectra and in magneto optical Kerr effect measurements (Figures S8 and S9 in Supporting Information).

We believe the interface engineering demonstrated here is not limited to STO substrates but also can be tailored to STO buffer layers on various perovskite substrates with different lattice parameters. To extend our approach, we tested STO-buffered $(La,Sr)(Al,Ta)O_3$ (LSAT) substrates with pure TiO_2- and mixed-terminations. Temperature-dependent resistivity of Ba-122 shows that T_c values are 18.8 and 17.0 K in TiO_2- and mixed-terminations, respectively (Figure S10 in Supporting Information). The T_c trend in STO-buffered system is similar to the result in STO substrate with the same film thickness of Ba-122.

Conclusions. We have determined the interfacial atomic configurations in Co-doped $BaFe_2As_2$ epitaxial thin films on both TiO_2- and SrO-terminated (001) $SrTiO_3$ substrates by using first-principles calculations and high-resolution scanning transmission electron microscopy imaging. Co-doped Ba-122 thin films on TiO_2-terminated STO substrates show tetragonal structure with atomically sharp interfaces. In contrast, Co-doped $BaFe_2As_2$ on SrO-terminated $SrTiO_3$ has a monoclinic distortion with a $BaFeO_{3-x}$ intermediate layer. We have also found that the distinctively different interfacial structures strongly influence on superconducting transition temperatures of Ba-122 ultrathin films depending on the surface terminations of (001) $SrTiO_3$ substrates. The control of interfacial atomic configurations by designing the topmost layer of the substrate is a novel approach to study interfacial superconductivity in Fe-based superconductors. We believe that this approach can open up many possibilities to explore the relationship between structure and property in Fe-based superconducting thin films.

■ ASSOCIATED CONTENT

Supporting Information

The Supporting Information is available free of charge on the ACS Publications website at DOI: 10.1021/acs.nanolett.8b02704.

Sample preparation, STEM HAADF imaging, theoretical calculation methods, EELS spectra, RHEED monitoring, AFM images, normalized resistivity for RRR extraction, XRD patterns, magnetic moment by SQUID, X-ray magnetic circular dichroism, magneto optical Kerr effect, and additional transport data (PDF)

■ AUTHOR INFORMATION

Corresponding Author

*E-mail: eom@engr.wisc.edu.

ORCID

Yi Wang: 0000-0001-6154-945X

Chang-Beom Eom: 0000-0002-8854-1439

Present Address

○(L.X.) Department of Physics, Southern University of Science and Technology, Shenzhen, Guangdong 518055, People's Republic of China.

Author Contributions

The manuscript was written through contributions of all authors. All authors have given approval to the final version of the manuscript.

Notes

The authors declare no competing financial interest.

■ ACKNOWLEDGMENTS

This work was supported by the U.S. Department of Energy (DOE), Office of Science, Office of Basic Energy Sciences (BES), under award number DE-FG02-06ER46327. The work at Penn State was supported by the U.S. Department of Energy, Office of Basic Energy Sciences, Division of Materials Sciences and Engineering under Award DE-FG02-07ER46417 (Y.W. and L.Q.C) and by National Science Foundation (NSF) through Grant No. CHE-1230924 (Z.K.L.). First-principles calculations were carried out on the resources of NERSC supported by the Office of Science of the U.S. Department of Energy under Contract No. DE-AC02-05CH11231. This research used resources of the Advanced Photon Source, a U.S. Department of Energy (DOE) Office of Science User Facility operated for the DOE Office of Science by Argonne National Laboratory under Contract No. DE-AC02-06CH11357. The work at UC Irvine was supported by the Department of Energy (DOE), Office of Basic Energy Sciences, Division of Materials Sciences and Engineering under Grant DE-SC0014430. The work at the National High Magnetic Laboratory was supported by National Science Foundation through grant No. DMR-1306785, DMR-1157490 and DMR-1644779 and by the State of Florida, USA.

DOI: 10.1021/acs.nanolett.8b02704
Nano Lett. 2018, 18, 6347−6352

REFERENCES

(1) Kamihara, Y.; Watanabe, T.; Hirano, M.; Hosono, H. Iron-based layered superconductor La[$O_{1-x}F_x$]FeAs (x = 0.05−0.12) with T_c = 26 K. *J. Am. Chem. Soc.* **2008**, *130*, 3296−3297.

(2) Fernandes, R. M.; Chubukov, A. V.; Schmalian, J. What drives nematic order in iron-based superconductors? *Nat. Phys.* **2014**, *10*, 97−104.

(3) Hunte, F.; Jaroszynski, J.; Gurevich, A.; Larbalestier, D. C.; Jin, R.; Sefat, A. S.; McGuire, M. A.; Sales, B. C.; Christen, D. K.; Mandrus, D. Two-band superconductivity in $LaFeAsO_{0.89}F_{0.11}$ at very high magnetic fields. *Nature* **2008**, *453*, 903−905.

(4) Lee, S.; Jiang, J.; Zhang, Y.; Bark, C. W.; Weiss, J. D.; Tarantini, C.; Nelson, C. T.; Jang, H. W.; Folkman, C. M.; Baek, S. H.; Polyanskii, A.; Abraimov, D.; Yamamoto, A.; Park, J. W.; Pan, X. Q.; Hellstrom, E. E.; Larbalestier, D. C.; Eom, C. B. Template engineering of Co-doped $BaFe_2As_2$ single-crystal thin films. *Nat. Mater.* **2010**, *9*, 397−402.

(5) Putti, M.; Pallecchi, I.; Bellingeri, E.; Cimberle, M. R.; Tropeano, M.; Ferdeghini, C.; Palenzona, A.; Tarantini, C.; Yamamoto, A.; Jiang, J.; Jaroszynski, J.; Kametani, F.; Abraimov, D.; Polyanskii, A.; Weiss, J. D.; Hellstrom, E. E.; Gurevich, A.; Larbalestier, D. C.; Jin, R.; Sales, B. C.; Sefat, A. S.; McGuire, M. A.; Mandrus, D.; Cheng, P.; Jia, Y.; Wen, H. H.; Lee, S.; Eom, C. B. New Fe-based superconductors: properties relevant for applications. *Supercond. Sci. Technol.* **2010**, *23*, 034003.

(6) Shimoyama, J. Potentials of iron-based superconductors for practical future materials. *Supercond. Sci. Technol.* **2014**, *27*, 044002.

(7) Yuan, H. Q.; Singleton, J.; Balakirev, F. F.; Baily, S. A.; Chen, G. F.; Luo, J. L.; Wang, N. L. Nearly isotropic superconductivity in $(Ba,K)Fe_2As_2$. *Nature* **2009**, *457*, 565−568.

(8) Zhao, J.; Huang, Q.; de la Cruz, C.; Li, S. L.; Lynn, J. W.; Chen, Y.; Green, M. A.; Chen, G. F.; Li, G.; Li, Z.; Luo, J. L.; Wang, N. L.; Dai, P. C. Structural and magnetic phase diagram of $CeFeAsO_{1-x}F_x$ and its relation to high-temperature superconductivity. *Nat. Mater.* **2008**, *7*, 953−959.

(9) Wang, F.; Lee, D. H. The electron-pairing mechanism of iron-based superconductors. *Science* **2011**, *332*, 200−204.

(10) Mizuguchi, Y.; Hara, Y.; Deguchi, K.; Tsuda, S.; Yamaguchi, T.; Takeda, K.; Kotegawa, H.; Tou, H.; Takano, Y. Anion height dependence of T_c for the Fe-based superconductor. *Supercond. Sci. Technol.* **2010**, *23*, 054013.

(11) Lee, C. H.; Iyo, A.; Eisaki, H.; Kito, H.; Fernandez-Diaz, M. T.; Ito, T.; Kihou, K.; Matsuhata, H.; Braden, M.; Yamada, K. Effect of structural parameters on superconductivity in fluorine-free LnFeAsO_{1-y} (Ln = La, Nd). *J. Phys. Soc. Jpn.* **2008**, *77*, 083704.

(12) Kimber, S. A. J.; Kreyssig, A.; Zhang, Y. Z.; Jeschke, H. O.; Valenti, R.; Yokaichiya, F.; Colombier, E.; Yan, J.; Hansen, T. C.; Chatterji, T.; McQueeney, R. J.; Canfield, P. C.; Goldman, A. I.; Argyriou, D. N. Similarities between structural distortions under pressure and chemical doping in superconducting $BaFe_2As_2$. *Nat. Mater.* **2009**, *8*, 471−475.

(13) Wu, J. J.; Lin, J. F.; Wang, X. C.; Liu, Q. Q.; Zhu, J. L.; Xiao, Y. M.; Chow, P.; Jin, C. Q. Pressure-decoupled magnetic and structural transitions of the parent compound of iron-based 122 superconductors $BaFe_2As_2$. *Proc. Natl. Acad. Sci. U. S. A.* **2013**, *110*, 17263−17266.

(14) Yamazaki, T.; Takeshita, N.; Kobayashi, R.; Fukazawa, H.; Kohori, Y.; Kihou, K.; Lee, C. H.; Kito, H.; Iyo, A.; Eisaki, H. Appearance of pressure-induced superconductivity in $BaFe_2As_2$ under hydrostatic conditions and its extremely high sensitivity to uniaxial stress. *Phys. Rev. B: Condens. Matter Mater. Phys.* **2010**, *81*, 224511.

(15) Okabe, H.; Takeshita, N.; Horigane, K.; Muranaka, T.; Akimitsu, J. Pressure-induced high-T_c superconducting phase in FeSe: Correlation between anion height and T_c. *Phys. Rev. B: Condens. Matter Mater. Phys.* **2010**, *81*, 205119.

(16) Tan, S. Y.; Zhang, Y.; Xia, M.; Ye, Z. R.; Chen, F.; Xie, X.; Peng, R.; Xu, D. F.; Fan, Q.; Xu, H. C.; Jiang, J.; Zhang, T.; Lai, X. C.; Xiang, T.; Hu, J. P.; Xie, B. P.; Feng, D. L. Interface-induced superconductivity and strain-dependent spin density waves in FeSe/$SrTiO_3$ thin films. *Nat. Mater.* **2013**, *12*, 634−640.

(17) Kawaguchi, T.; Sakagami, A.; Mori, Y.; Tabuchi, M.; Ujihara, T.; Takeda, Y.; Ikuta, H. The strain effect on the superconducting properties of $BaFe_2(As, P)_2$ thin films grown by molecular beam epitaxy. *Supercond. Sci. Technol.* **2014**, *27*, 065005.

(18) Ge, J. F.; Liu, Z. L.; Liu, C. H.; Gao, C. L.; Qian, D.; Xue, Q. K.; Liu, Y.; Jia, J. F. Superconductivity above 100 K in single-layer FeSe films on doped $SrTiO_3$. *Nat. Mater.* **2015**, *14*, 285−289.

(19) He, S. L.; He, J. F.; Zhang, W. H.; Zhao, L.; Liu, D. F.; Liu, X.; Mou, D. X.; Ou, Y. B.; Wang, Q. Y.; Li, Z.; Wang, L. L.; Peng, Y. Y.; Liu, Y.; Chen, C. Y.; Yu, L.; Liu, G. D.; Dong, X. L.; Zhang, J.; Chen, C. T.; Xu, Z. Y.; Chen, X.; Ma, X.; Xue, Q. K.; Zhou, X. J. Phase diagram and electronic indication of high-temperature superconductivity at 65 K in single-layer FeSe films. *Nat. Mater.* **2013**, *12*, 605−610.

(20) Lee, J. J.; Schmitt, F. T.; Moore, R. G.; Johnston, S.; Cui, Y. T.; Li, W.; Yi, M.; Liu, Z. K.; Hashimoto, M.; Zhang, Y.; Lu, D. H.; Devereaux, T. P.; Lee, D. H.; Shen, Z. X. Interfacial mode coupling as the origin of the enhancement of T_c in FeSe films on $SrTiO_3$. *Nature* **2014**, *515*, 245−248.

(21) Liu, D. F.; Zhang, W. H.; Mou, D. X.; He, J. F.; Ou, Y. B.; Wang, Q. Y.; Li, Z.; Wang, L. L.; Zhao, L.; He, S. L.; Peng, Y. Y.; Liu, X.; Chen, C. Y.; Yu, L.; Liu, G. D.; Dong, X. L.; Zhang, J.; Chen, C. T.; Xu, Z. Y.; Hu, J. P.; Chen, X.; Ma, X. C.; Xue, Q. K.; Zhou, X. J. Electronic origin of high-temperature superconductivity in single-layer FeSe superconductor. *Nat. Commun.* **2012**, *3*, 931.

(22) Wang, Q. Y.; Li, Z.; Zhang, W. H.; Zhang, Z. C.; Zhang, J. S.; Li, W.; Ding, H.; Ou, Y. B.; Deng, P.; Chang, K.; Wen, J.; Song, C. L.; He, K.; Jia, J. F.; Ji, S. H.; Wang, Y. Y.; Wang, L. L.; Chen, X.; Ma, X. C.; Xue, Q. K. Interface-induced high-temperature superconductivity in single unit-cell FeSe films on $SrTiO_3$. *Chin. Phys. Lett.* **2012**, *29*, 037402.

(23) Bozovic, I.; Ahn, C. A new frontier for superconductivity. *Nat. Phys.* **2014**, *10*, 892−895.

(24) Haindl, S.; Kidszun, M.; Oswald, S.; Hess, C.; Buchner, B.; Kolling, S.; Wilde, L.; Thersleff, T.; Yurchenko, V. V.; Jourdan, M.; Hiramatsu, H.; Hosono, H. Thin film growth of Fe-based superconductors: from fundamental properties to functional devices. A comparative review. *Rep. Prog. Phys.* **2014**, *77*, 046502.

(25) Hanawa, M.; Ichinose, A.; Komiya, S.; Tsukada, I.; Imai, Y.; Maeda, A. Empirical selection rule of substrate materials for iron chalcogenide superconducting thin films. *Jpn. J. Appl. Phys.* **2012**, *51*, 010104.

(26) Iida, K.; Hanisch, J.; Thersleff, T.; Kurth, F.; Kidszun, M.; Haindl, S.; Huhne, R.; Schultz, L.; Holzapfel, B. Scaling behavior of the critical current in clean epitaxial $Ba(Fe_{1-x}Co_x)_2As_2$ thin films. *Phys. Rev. B: Condens. Matter Mater. Phys.* **2010**, *81*, 100507R.

(27) Lee, S.; Tarantini, C.; Gao, P.; Jiang, J.; Weiss, J. D.; Kametani, F.; Folkman, C. M.; Zhang, Y.; Pan, X. Q.; Hellstrom, E. E.; Larbalestier, D. C.; Eom, C. B. Artificially engineered superlattices of pnictide superconductors. *Nat. Mater.* **2013**, *12*, 392−396.

(28) Tarantini, C.; Kametani, F.; Lee, S.; Jiang, J.; Weiss, J. D.; Jaroszynski, J.; Hellstrom, E. E.; Eom, C. B.; Larbalestier, D. C. Development of very high J_c in $Ba(Fe_{1-x}Co_x)_2As_2$ thin films grown on CaF_2. *Sci. Rep.* **2015**, *4*, 7305.

(29) Koster, G.; Kropman, B. L.; Rijnders, G. J. H. M.; Blank, D. H. A.; Rogalla, H. Quasi-ideal strontium titanate crystal surfaces through formation of strontium hydroxide. *Appl. Phys. Lett.* **1998**, *73*, 2920−2922.

(30) Clemens, O.; Groting, M.; Witte, R.; Perez-Mato, J. M.; Loho, C.; Berry, F. J.; Kruk, R.; Knight, K. S.; Wright, A. J.; Hahn, H.; Slater, P. R. Crystallographic and magnetic structure of the perovskite-type compound $BaFeO_{2.5}$: Unrivaled complexity in oxygen vacancy ordering. *Inorg. Chem.* **2014**, *53*, 5911−5921.

(31) Knochel, P. L.; Keenan, P. J.; Loho, C.; Reitz, C.; Witte, R.; Knight, K. S.; Wright, A. J.; Hahn, H.; Slater, P. R.; Clemens, O. Synthesis, structural characterisation and proton conduction of two new hydrated phases of barium ferrite $BaFeO_{2.5-x}(OH)_{2x}$. *J. Mater. Chem. A* **2016**, *4*, 3415−3430.

DOI: 10.1021/acs.nanolett.8b02704
Nano Lett. 2018, 18, 6347−6352

(32) Tan, H.; Verbeeck, J.; Abakumov, A.; Tendeloo, G. V. Oxidation state and chemical shift investigation in transition metal oxides by EELS. *Ultramicroscopy* **2012**, *116*, 24−33.
(33) Kourkoutis, L. F.; Xin, H. L.; Higuchi, T.; Hotta, Y.; Lee, J. H.; Hikita, Y.; Schlom, D. G.; Hwang, H. Y.; Muller, D. A. Atomic-resolution spectroscopic imaging of oxide interfaces. *Philos. Mag.* **2010**, *90*, 4731−4749.
(34) Sanchez, F.; Ocal, C.; Fontcuberta, J. Tailored surfaces of perovskite oxide substrates for conducted growth of thin films. *Chem. Soc. Rev.* **2014**, *43*, 2272−2285.

DOI: 10.1021/acs.nanolett.8b02704
Nano Lett. 2018, 18, 6347−6352